Size- and shape-dependent foreign body immune response to materials implanted in rodents and non-human primates

HHS Public Access

Author manuscript

Nat Mater. Author manuscript; available in PMC 2015 December 01.

Published in final edited form as:

Nat Mater. 2015 June ; 14(6): 643–651. doi:10.1038/nmat4290.

Size- and shape-dependent foreign body immune response to materials implanted in rodents and non-human primates

Omid Veiseh[*,1,2,3], **Joshua C. Doloff**[*,1,3], **Minglin Ma**[*,1,3,4], **Arturo J. Vegas**[1,3], **Hok Hei Tam**[1,2], **Andrew R. Bader**[1,3], **Jie Li**[1,3], **Erin Langan**[1,3], **Jeffrey Wyckoff**[1], **Whitney S. Loo**[2], **Siddharth Jhunjhunwala**[1,3], **Alan Chiu**[1,3], **Sean Siebert**[1,3], **Katherine Tang**[1,3], **Jennifer Hollister-Lock**[5], **Stephanie Aresta-Dasilva**[1,3], **Matthew Bochenek**[6], **Joshua Mendoza-Elias**[6], **Yong Wang**[6], **Merigeng Qi**[6], **Danya M. Lavin**[1,3], **Michael Chen**[1,3], **Nimit Dholakia**[1,3], **Raj Thakrar**[1,3], **Igor Lacík**[7], **Gordon C. Weir**[5], **Jose Oberholzer**[6], **Dale L. Greiner**[8], **Robert Langer**[1,2,3,9,10,11], and **Daniel G. Anderson**[1,2,3,9,10,11,#]

[1]David H Koch Institute for Integrative Cancer Research, Massachusetts Institute of Technology, 500 Main Street, Cambridge, MA, 02139, USA

[2]Department of Chemical Engineering, Massachusetts Institute of Technology, 77 Massachusetts Avenue, Cambridge, MA, 02139, USA

[3]Department of Anesthesiology, Boston Children's Hospital, 300 Longwood Ave, Boston, MA 02115, USA

[5]Section on Islet Cell and Regenerative Biology, Research Division, Joslin Diabetes Center, One Joslin Place, Boston, MA 02215, USA

[6]Division of Transplantation, Department of Surgery, University of Illinois at Chicago, Chicago, IL

[7]Department for Biomaterials Research, Polymer Institute of the Slovak Academy of Sciences, Dubravska cesta 9, 845 41 Bratislava, Slovakia

[8]Program in Molecular Medicine, University of Massachusetts Medical School, Worcester, MA 01605, USA

[#]dgander@mit.edu; Tel.: +1 617 258 6843; fax: +1 617 258 8827.

[*]Equal contributing authors

[4]Current address: Biological and Environmental Engineering, Cornell University, Ithaca, NY 14853, USA

AUTHOR CONTRIBUTIONS

O.V., J.D., M.M. and D.A. conceived idea, designed experiments, analyzed data, and wrote the manuscript. O.V., J.D., M.M. A.V., A.B., J.L., E.L., J.W., W.L., S.J., A.C., S.S., K.T., J.H-L., S.A-D., M.B., J.M-E., Y.W., M.Q., D.L., M.C, N.D., R.T., I.L., G.W., and J.O., performed experiments. H.T. performed statistical analyses of data sets and aided in the preparation of displays communicating data sets. G.W., J.O., and D.G. provided conceptual advice and technical support. R.L. and D.A. supervised the study. All authors discussed the results and assisted in the preparation of the manuscript.

Competing Financial Interests

The authors declare no competing financial interests.

SUPPLEMENTARY INFORMATION

Supplementary Methods and Materials
Supplementary Discussion
Supplementary Table 1 and 2
Supplementary Figure S1–S17
Supplemental videos V1–V8

[9]Division of Health Science Technology, Massachusetts Institute of Technology, 77 Massachusetts Avenue, Cambridge, MA, 02139, USA

[10]Institute for Medical Engineering and Science, Massachusetts Institute of Technology, 77 Massachusetts Avenue, Cambridge, MA, 02139, USA

[11]Harvard-MIT Division of Health Science and Technology, Massachusetts Institute of Technology, 77 Massachusetts Avenue, Cambridge, MA, 02139, USA

Abstract

The efficacy of implanted biomedical devices is often compromised by host recognition and subsequent foreign body responses. Here, we demonstrate the role of the geometry of implanted materials on their biocompatibility in vivo. In rodent and non-human primate animal models, implanted spheres 1.5 mm and above in diameter across a broad spectrum of materials, including hydrogels, ceramics, metals, and plastics, significantly abrogated foreign body reactions and fibrosis when compared to smaller spheres. We also show that for encapsulated rat pancreatic islet cells transplanted into streptozotocin-treated diabetic C57BL/6 mice, islets prepared in 1.5 mm alginate capsules were able to restore blood-glucose control for up to 180 days, a period more than 5-fold longer than for transplanted grafts encapsulated within conventionally sized 0.5-mm alginate capsules. Our findings suggest that the in vivo biocompatibility of biomedical devices can be significantly improved by simply tuning their spherical dimensions.

Biomaterials and devices implanted in the body are used for a broad spectrum of clinical applications including cell transplantation[1], controlled drug release[2], continuous sensing and monitoring of physiological conditions[3], electronic pacing[4], and tissue regeneration[5]. For many of these applications the performance of the device is dependent on its interaction with the host immune system[6]. Immune recognition initiates a cascade of cellular processes leading to foreign body reactions, which include persistent inflammation, formation of foreign body giant cells (fused macrophages), fibrosis (walling-off), and damage to the surrounding tissue[7, 8]. Even when devices are prepared using non-reactive biomaterials, a 100-μm thick fibrotic tissue often builds up (< 1 month), enveloping the implanted device[9]. These unwanted effects can be both deleterious to the function of the device and a cause of significant pain and discomfort for the patient[9, 10].

In attempting to develop more biocompatible materials and devices, researchers have investigated a range of parameters including tuning material physiochemical properties to limit protein fouling[11, 12], applying cell-resistive coatings[13], modifying surfaces with ligands to selectively modulate immune cell recruitment[14, 15], and controlling surface porosity[16]. However, only a limited number of studies have examined the role of material or device geometry on modulating foreign body responses and fibrosis[17, 18, 19, 20]. Malaga et al. evaluated six various medical-grade polymers which were extruded into geometries of rods with circular-, triangular-, and pentagonal-shaped cross sections, and then implanted these materials into rat gluteal muscles for 14 days[19]. Among the shapes tested, circular rods produced the least amount of foreign body responses followed by pentagonal, and then triangular. Salthouse et al. described that implant shape can profoundly affect macrophage behavior at the interface of percutaneous implants and observed that smooth, well contoured

implants with no acute angles are more biocompatible[20]. Since these notable studies it has long been accepted that indeed materials with smooth surfaces are likely to be more biocompatible than those with sharp edges[19], however there is still no consensus on an ideal geometry[21].

Surface porosity has also been identified as an influential parameter affecting angiogenesis[16, 22]. Brauker et al. evaluated the role of surface porosity in promoting angiogenesis by comparing polytetrafluoroethylene (PTFE) membranes with 5-micron-pore-sizes to ones with 0.02-micron-pore-sizes[22]. Their study demonstrated that the larger pore membranes had 80–100-fold more vascular structures associated with the implant. More recently, Madden et al. studied a larger range of pore sizes (0 – 80 μm) and demonstrated that an even stronger angiogenic response could be produced by tuning the pore sizes specifically to 30–40 μm[16].

At the macro level (>100 μm in size), it is generally held that thicker materials produce a proportionally higher magnitude of foreign body responses and fibrosis[3, 21]. Ward et al. examined the influence of material size by comparing host response to polyurethane substrates prepared as cylinders that were either 300 or 2000 μm in diameter. They found that increasing the size of implanted materials resulted in larger foreign body reactions, and the formation of a thicker layer of fibrosis around the implant[23]. Interestingly, to our knowledge no one has studied the effect of sphere diameter on biocompatibility.

In this study, we sought to examine the role of spherical biomaterial geometry on biocompatibility in vivo. Our initial work focused on interrogating immune response and fibrosis upon implantation of alginate hydrogels. Commonly prepared as microspheres of 100 – 1000 μm in diameter, alginate hydrogels are widely used for a number of *in vivo* applications including controlled drug release, tissue regeneration, and immunoisolation of therapeutic cells[24, 25]. One biomedical application for which alginate microspheres (0.3–1 mm in diameter) have been extensively evaluated is the immunoisolation of donor pancreatic islets for the treatment of Type-1 diabetes[1, 26]. Host recognition and fibrosis of alginate capsules in humans, independent of donor tissue, is the key barrier to the clinical translation of encapsulated donor islets for treatment of type-1 diabetes[26, 27, 28]. When implanted into the intraperitoneal space of non-human primates or immunocompetent rodents, alginate microspheres elicit foreign body reactions and fibrosis[29, 30]. To ensure proper biocompatibility assessment in our studies we used an immunocompetent C57BL/6 mouse model for our initial screening, because this strain is known to produce a strong fibrotic and foreign body response similar to observations made in human patients[31].

To investigate the effect of sphere diameter on biocompatibility we fabricated Ba^{+}-cross-linked SLG20 alginate hydrogel spheres in eight different sizes, 0.3 mm, 0.4 mm, 0.5 mm, 0.7 mm, 0.9 mm, 1 mm, 1.5, and 1.9 mm, with very narrow size distributions (Supplementary Figure S1). These spheres (350 μl/mouse) were then implanted into the intraperitoneal space of C57BL/6 mice, where they were retained for 14 days. After this period, spheres were harvested from sacrificed mice and then studied for cellular deposition and fibrosis (Figure 1). Dark field phase contrast images from retrieved spheres show a marked reduction in cellular deposition onto spheres as their size is increased (Figure 1a).

Cellular deposition on spheres was examined using Z-stacked confocal imaging using DAPI (nucleus marker), F-actin (cellular cytoskeleton marker), and alpha-smooth muscle actin (α-SMA, myofibroblast marker). Interestingly, the larger spheres had significantly reduced fibrotic deposition (Figure 1b and Supplemental Figure S2). Additional immunostaining for the host immune cell markers CD68 (macrophage), Ly6G/Ly6C-GR1 (neutrophil), and TGF-β (inflammation marker) also showed reduced immune cell deposition on larger spheres (Supplemental Figure S3). q-PCR expression analysis of additional fibrosis markers, namely collagen 1a1 (Col1a1), collagen 1a2 (Col1a2), and αSMA, further indicated reduced cellular deposition as the sphere size was increased (Figure 1c–e). Western blot analysis of α-SMA expression within the cellular overgrowth on spheres showed a significant decrease as sphere size was increased (Figure 1f and g).

To ensure that the size-modulated fibrotic response effect is not simply a function of surface area, we implanted spheres of two sizes, 0.5 mm and 1.5 mm, normalized in total surface area. In other words, 100 μl/mouse of medium sized and 300 μl/mouse of large sized spheres were implanted into the intraperitoneal space of C57BL/6 mice and then retrieved after 14 days. Dark field phase contrast images of the retrieved spheres revealed only limited cellular deposition on the 1.5 mm-sized spheres and significant cellular deposition on the 0.5 mm sized spheres (Supplemental Figure S4). These findings indicate that the phenomenon is size-mediated and independent of total surface of area of implanted material.

We next evaluated whether the effects of implant size on fibrosis are related to a delay in the kinetics of cellular deposition on the larger sized spheres. To study this hypothesis, 0.3 mm and 1.5 mm-sized SLG20 alginate hydrogel spheres were implanted into the intraperitoneal space of C57BL/6 mice for a significantly longer period of 6 months. After 6 months the implanted hydrogel spheres were retrieved and examined for cellular deposition. Dark field phase contrast images from retrieved capsules show that the 1.5 mm spheres are largely devoid of cellular deposition while the 0.3 mm sized spheres are covered with deposited cells and are clumped together in fibrotic tissue (Supplemental Figure S5).

We also asked whether or not this size-modulated fibrotic deposition phenomenon would extend to other materials known to produce higher levels of fibrotic reactions upon implantation. To this end, we implanted a medium sized (0.4–0.6 mm) and larger (1.5–2.5 mm) sized spheres composed of SLG20 alginate (sterile grade alginate), LF10/60 alginate (pharmaceutical grade alginate), stainless steel, glass, polycaprolactone, and polystyrene into the intraperitoneal space of C57BL/6 mice. The surface roughness of material spheres we evaluated here only included relatively smooth surfaced materials (<1 μm roughness)[32, 33]. Bright-field images from retrieved materials 14 days post-implant revealed significant cellular deposition on the medium-sized versions of all materials tested. Interestingly, all materials tested at an increased size led to a marked reduction of the thickness of cellular overgrowth deposition (Figure 2a). Immunofluorescence stained z-stacked confocal images of retrieved materials showed a significant decrease in macrophage (CD68) and myofibroblast (αSMA) deposition across all materials tested, and significantly, large SLG20 alginate, LF10/60 (endotoxin containing alginate), glass, and stainless steel spheres had negligible cellular deposition (Figure 2b).

To further evaluate the innate immune response to spheres of different sizes, we collected and analyzed the omental and epididymal fat pad tissue peripheral to the implants for innate immune cell infiltration, using a combination of flow cytometry (Figure 2c and d) and q-PCR analysis (Supplemental Figure S6). These analyses revealed that across all materials tested (SLG20 alginate, LF10/60 alginate, stainless steel, glass, polycaprolactone, and polystyrene) increasing sphere size led to a significant reduction of innate immune cell accumulation in peripheral tissue. These findings were further validated through a multiplexed inflammatory mouse cytokine profile (Figure 2e). Notably, our evaluation of a spectrum of materials with a range of mechanical stiffness properties varying from soft (Alginate hydrogels, < 100 kPa)[34] to hard (Stainless steel, 100s of GPa)[35] demonstrates that size and shape rather than stiffness plays a critical role in biocompatibility.

We next sought to examine whether this observed size-modulated fibrotic effect would translate to a larger rodent model. To examine this, we implanted 0.5 mm and 2.0 mm glass spheres into the intraperitoneal space of Sprague-Dawley rats and then retrieved the materials after 14 days. Bright field and Z-stacked confocal images obtained from retrieved glass microspheres show that the large spheres are devoid of any cellular deposition while the smaller spheres are significantly clumped together and embedded within a thick fibrotic capsule (Supplemental Figure S7a and b). q-PCR expression analysis of fibrosis markers, collagen 1a1 (Col1a1), collagen 1a2 (Col1a2), and αSMA, verified that increasing sphere size resulted in a significant reduction of fibrosis formation directly on spheres (Supplemental Figure S7c). These results suggest our size-dependent fibrotic response observations in C57BL/6 mice also translate to other larger rodent species.

Next, we wanted to study if these findings could translate to higher order species and also to other implant sites. To evaluate this, we implanted SLG20 alginate hydrogels, prepared as 0.5 mm and 1.5 mm spheres (N = 4) as well as cylinders (4 mm diameter x 1 mm height) (N = 2), subcutaneously into the dorsal regions of non-human primates (NHPs) for either 14 or 28 days. At both 14 and 28 days post implantation retrieval time points the 1.5 mm-sized SLG20 alginate spheres were not embedded in host tissue and freely dissociated from the implant site upon incision with a biopsy punch (Figure 4a and Supplemental Figure S8). The retrieved 1.5 mm spheres visually appeared to be translucent and void of cellular overgrowth (Figure 4b and Supplemental Figure S8). H&E stained sections of retrieved large spheres confirmed negligible cellular deposition and a lack of fibrosis (Figure 4c). Conversely, at both 14 and 28-day retrieval time points, the implanted 0.5 mm sized spheres and cylinders were profusely embedded in host tissues (Supplemental Figure S8). Excised tissue obtained from the implant sites of SLG20 alginate 1.5 mm spheres, 0.5 mm spheres, cylinders, and saline injected control tissue were examined through histological analysis using a combination of H&E and Masson's Trichrome staining (Figure 4d). The obtained images confirm the lack of large sphere embedding or fibrosis. However, extensive embedding and fibrosis buildup (up to 100 μm thick) is visible enveloping the implanted cylinders and medium sized spheres.

To confirm that the subcutaneous dorsal NHP observations could also translate to the intraperitoneal site of NHPs, a smaller pilot study was performed, in which 0.5 mm and 1.5 mm sized spheres of SLG20 alginate hydrogels were separately implanted into non-human

primates (n = 1 per treatment) using a minimally invasive laparoscopic procedure (Supplemental Figure S9)[36]. A laparoscopic camera was used to capture images and video of the spheres immediately after and also again at 14 days post implantation. The obtained in situ images reveal that the 1.5 mm-sized spheres remain translucent and are not embedded into host omentum/fat tissue after 14 days; conversely, the 0.5 mm sized spheres are impeded in to the omentum/fat tissue (Supplemental Figure S9a). An IP lavage with saline at 14 days post implantation enabled retrieval of SLG20 1.5 mm spheres, however the 0.5 mm sized spheres could not be retrieved because of strong adherence and embedding into the IP host tissue (omentum) (Supplemental Videos V1 and V2). The retrieved 1.5 mm spheres were examined using dark field imaging and appear to be transparent with negligible cellular overgrowth (Supplemental Figure S9b). Z-stacked confocal imaging of the retrieved 1.5 mm spheres confirms minimal cellular deposition, a lack of immune macrophages, and fibrosis-associated activated myofibroblast coverage (Supplemental Figure S9c). To verify the embedding of the 0.5 mm-sized spheres within the NHP omentum, a biopsy punch was used to excise a sample of this tissue for histological analysis, which confirmed their embedding, and significant fibrotic tissue buildup was observed enveloping the medium sized spheres (Supplemental Figure S9d).

To highlight the implications of our findings we investigated whether the improvements we observed in biocompatibility through the tuning of material geometry could produce improved/prolong function of an implanted biomedical device. To study this effect, we evaluated the survival of Islets of Langerhans (islets) immunoisolated/encapsulated within conventionally sized alginate microcapsules 0.5 mm compared to islets protected within a 1.5 mm sized capsule. Previously, we and others have shown that host recognition and fibrosis via cellular and collagen deposition on the surface of transplanted 0.5 mm sized alginate microcapsules results in encapsulated islet graft cell death and the failure of diabetic correction in STZ-treated C57BL/6 mice[28, 37, 38]. Notably, in the context of islet encapsulation, the diameter of the hydrogel capsules is a parameter that has been largely overlooked and based on our observations it could play an important role in improving the efficacy of the transplanted grafts[39]. Furthermore, it has been traditionally assumed that small capsules (< 350 μm) allows better diffusion and transportation of nutrients and oxygen to the encapsulated islets compared to medium (350–700 μm) and larger capsules (>700 μm)[40]. Thus, to our knowledge larger 1.5 mm sized spherical capsules have previously not been evaluated for islet cell encapsulation.

Using a xenogeneic treatment model of transplanting rat pancreatic islets into STZ-induced diabetic C57BL/6 mice we investigated the role of capsule size on cell survival. Rat islets (500 IE per mouse) were separately encapsulated into SLG20 alginate hydrogels prepared as 1.5 mm, or 0.5 mm spheres. For these studies we used an islet density preparation of 500 IE per 0.325 ml alginate solution because at this density we observed very few protrusions of islets outside of capsules. Live/dead staining was used to confirm the viability of islets after encapsulation (Figure 4a). To investigate potential diffusion barriers due to using larger sized 1.5 mm capsules, prior to transplantation, we evaluated the kinetics of both glucose and insulin diffusion within 1.5 mm and 0.5 mm capsules loaded with islets. We observed no significant differences in diffusion kinetics of glucose (Supplemental Figure S10) or insulin (Supplemental Figure S11) as a function of capsule geometry (Supplemental

Discussion). After transplantation, blood glucose (BG) correction was used as an indicator to non-invasively monitor cell graft function over time and measurements were taken at least 3 times a week. All mice (n = 5) in the 0.5 mm capsule group failed (i.e. BG above 200 mg/dl for 3 consecutive measurements), on average, by 30 days following transplantation, while in the 1.5 mm capsule group (n = 5), stayed cured, on average, even until 175 days (greater than a 5-fold increase) post-transplantation, when the experiment was stopped (Supplemental Figure S12). The difference in both BG normalization (Figure 4b) and fraction cured (Figure 4d) was significantly different ($p<0.0001$) between the 0.5 mm and 1.5 mm capsule groups following the initial failure in regulating BGs by the 0.5 mm group (~day 25) throughout the remainder of the experiment. At 7 days post-transplantation a glucose tolerance test (GTT) was used to evaluate the kinetics of blood glucose correction and no significant delays were measured as a function of capsule geometry (Figure 4c).

Upon termination of this study, 6 months post-transplantation, capsules were retrieved and analyzed for fibrosis and presence of viable islets. Dark field imaging revealed that the 0.5 mm capsules were covered in cellular deposition and clumped but the 1.5 mm capsules were largely clean and void of cellular deposition (Figure 4e). Confocal images acquired from retrieved 0.5 mm and 1.5 mm capsules showed positive Newport Green (islet viability marker) staining only in the 1.5 mm group (Figure 4f). Western blot assays were additionally performed on extracted proteins from retrieved capsules in each group to monitor relative expression of PDX-1 (islet viability marker) and alpha smooth muscle actin (fibrosis marker). For this assay, approximately 50% of capsules retrieved from each mouse was digested and processed for total protein extraction. 4 out of 5 mice in the 0.5 mm capsule group had comparatively diminished PDX-1 expression and all 5 mice showed high levels of alpha smooth muscle expression; conversely, high levels of PDX-1 and minimal alpha smooth muscle actin were detected in capsules retrieved from all 5 mice in the 1.5 mm capsule group (Figure 4g). PDX1 expression results were further verified using qPCR analysis of RNA isolated from retrieved capsules, and an ~8-fold higher levels of rat Pdx1 was detectable in the 1.5 mm capsules compared to 0.5 mm capsules group (Figure 4h). Combined our results suggest that grafts in 1.5 mm-sized capsules survived ~ 6 fold prolonged duration compared to those prepared in conventionally sized 0.5 mm capsules because the tuned geometry hydrogels were able to resists fibrosis for a longer duration. Interestingly, while we did not observe significant buildup of fibrosis on the capsules upon retrieval after 180 days, however the mice in this treatment group lost blood glucose control after approximately 140 days. This likely suggests some islet viability loss after transplantation, which could be related to the long-term durability of the rat islets used in this treatment model.

To better understand innate immune response as a function of implant size, we conducted a kinetic profiling analysis of host-mediated innate immune recognition following implantation of 0.5 mm and 1.5 mm-sized SLG20 alginate spheres, over a 28-day period (Figure 5) in C57BL/6 mice. Flow cytometry was used to quantify the accumulation of myeloid cells (Figure 5a), neutrophils (Figure 5b), and macrophages (Figure 5c) directly on spheres of 0.5 mm and 1.5 mm sizes at 1, 4, 7, 14, and 28 days post-implant. At all time points evaluated, we observed a significant increase in the accumulation of myeloid cells onto 0.5 mm-sized spheres compared to the 1.5 mm-sized spheres (Figure 5a). In probing

macrophage and neutrophil cells, by four days post-implantation we observed significantly increased accumulation on 0.5 mm-sized spheres, which appears to plateau by day 7 (Figure 5b and c). Notably, on 1.5 mm-sized spheres we observed negligible numbers of neutrophil cells and a limited number of myeloid and macrophage cells at all time points.

Macrophages have been implicated as key drivers of the foreign-body reaction to implanted materials[41]. To probe their role towards the fibrotic responses to the implanted materials we performed a series of experiments in which we transplanted SLG20 alginate spheres into the IP space of a transgenic mouse model, MAFIA, which enables the induction of macrophage cell depletion. In this model, a macrophage Fas-induced apoptosis transgene enable inducible/reversible apoptosis of macrophages using the mouse colony stimulating factor 1 receptor promoter (Csf1r) to drive expression of a mutant human FK506 binding protein 1A, 12kDa[42]. Furthermore, an EGFP transgene included in this model enables the in situ fluorescent monitoring of macrophage cells[42].

First, to confirm the importance of macrophages in driving the fibrosis responses we transplanted 0.5 mm-sized SLG20 spheres into the IP space of MAFIA mice treated to induce depletion of macrophages and also as a control into MAFIA mice without depletion for 14 days. Dark field microscope images of the retrieved spheres revealed only limited cellular deposition onto spheres implanted in mice with depleted macrophages and conversely significant cellular deposition onto spheres received from mice with macrophages (Supplemental Figure S13). These results confirm that macrophages are indeed a key driver of the fibrotic responses we have observed in response to our transplanted materials.

Second, to monitor macrophage behavior in real-time, we performed *in vivo* intravital imaging on implanted alginate spheres of 0.5 mm and 1.5 mm size, which were fluorescently labeled. Spherical implants were studied in the IP space of MAFIA mice (Supplemental Figure S14). In vivo Z-stacked intravital images obtained from implanted medium- and large-sized spheres at 1, 4, and 7 days post-implant indicate that macrophage cells extravasate from peripheral fat pad tissue and accumulate onto 0.5 mm spheres over that one week period, while very few macrophages can be observed near the 1.5 mm spheres (Figure 5d). Z-stacked and time lapse intravital images of macrophage accumulation onto 0.5 mm and 1.5 mm sized spheres at 1, 4, and 7 days post-implantation confirm both a lack of macrophage activity and numbers surrounding 1.5 mm size spheres, and significant macrophage activity and numbers around 0.5 mm sized spheres (Supplemental Videos V3–V8). We hypothesized that since the 1.5 mm spheres are surrounded by only a few macrophage cells, the macrophages around the large spheres are not becoming activated, resulting in reduced recruitment and extravasation of additional macrophages.

Macrophage cells have remarkable plasticity that allows them to efficiently respond to environmental signals and change their phenotype to address the implicated stimuli[43]. There is a broad spectrum of macrophage activations which can be categorized into three states namely, classical activation (pro-inflammatory, $M_{Classic}$), alternative activation (pro-healing, M_{Wound}), and regulatory activation (M_{Reg})[44]. These phenotypes can be characterized through gene expression analysis of specific markers that correlate with each activation

state[45]. A pro-inflammatory macrophage phenotype correlates with elevated expression of Tumor Necrosis Factor α (TNF α), Interleukin 1 (IL1), and Interferon Regulatory Factor 5 (IRF5)[44, 45, 46]. A pro-wound healing phenotype of macrophage correlates with up regulation in expression of Dendritic Cell Immune Receptor (Dcir), Stabilin 1 (Stab1), chemokine (C-C motif) ligand 22 (CCL22), Chitinase-like 3 (YM1), and Arginase 1 (Arg1)[44, 45, 46]. Meanwhile, a regulatory macrophage phenotype has been characterized to correlate with elevated expression of Interleukin 10 (IL10), TNF superfamily member 14 (Light), and Sphingosine Kinase 1 (Sphk1)[44, 45, 46]. To elucidate the changing activation/differentiation states of macrophages we examined a range of implanted constructs using a series of markers reflecting $M_{Classic,}$ M_{Wound}, and M_{Reg} phenotypes[41, 43, 44, 46]. At 1, 4, and 7 days post-implantation, gene expression analysis was used to probe phenotype marker expression of cells isolated from the intraperitoneal space, omental fat pad tissue, and directly on spheres. Overall, we observed significantly different gene expression patterns for cells associated with these tissues following implantation of 0.5 mm-sized spheres when compared to 1.5 mm-sized spheres (Supplemental Table S1).

Implantation of both 0.5 mm- and 1.5 mm-sized spheres resulted in an increased expression of markers associated with a wound healing phenotype in the intraperitoneal and peripheral omentum fat compartments (Supplemental Figures S15 and S16, and Supplemental Table S1). This phenotype was elevated at day 4 for both sizes of spheres implanted in mice, and decreased by day 7 for the 1.5 mm-sized spheres. We believe that these data are consistent with macrophage activation in these compartments, that is reduced when the implanted material are 1.5 mm spheres. Fibrotic tissue obtained directly from the 0.5 mm-sized s showed increasing expression of markers associated with all three macrophage phenotypes. In contrast, expression of macrophage markers associated only with classical and wound-healing phenotypes was enriched on 1.5-mm spheres (Figure 5e and Supplemental Table S1). Regulatory macrophage markers were not significantly up-regulated at any time point or in any compartment tested following implantation of 1.5 mm-sized spheres. However, increased expression of markers associated with this macrophage phenotype was observed on days 4 and 7 in cells associated with the 0.5 mm spheres (Figure 5e). Combined our observations suggest that a lack of regulatory macrophage cell accumulation on large size spheres correlates with the truncated fibrosis responses.

In summary, we have demonstrated that tuning the geometry of implanted materials we can influence their host recognition and propagation of foreign body reactions. Spherical materials that are of 1.5 mm in diameter or greater proved to be significantly more biocompatible compared to their smaller-sized or counterparts. This effect was demonstrated to be independent of total implanted surface area and visible with all materials tested. Further, our finding suggests that simply increasing implant size is insufficient to resist foreign body responses and that a spherical shape is also integral for resisting host fibrosis/rejection. Significantly, alginate microspheres of 1.5 mm in diameter demonstrated an ability to ward off cellular deposition for at least 6 months. Modulating the spherical dimensions of a broad spectrum of materials encompassing hydrogels, ceramics, metals, and plastics also showed that spheres of 1.5 mm in diameter or greater significantly mitigated foreign reactions and fibrosis. We believe these findings have important implications for the design of in vivo-implanted biomedical devices for a range of applications including cell

transplantation, controlled drug release, implantable sensors, and prosthesis for tissue engineering.

Materials and Methods

Detailed description of methods and any associated references are available in the online version of the paper. In brief, all materials were implanted intraperitoneally or subcutaneously into and retrieved at specified times from C57BL/6 mice, C57BL/6-Tg(Csf1r-EGFP-NGFR/FKBP1A/TNFRSF6)2Bck/J mice, Sprague-Dawley rats, or cynomolgus macaques non-human primates in accordance with approved protocols and federal guidelines. Sample processing, staining, FACS, NanoString expression analysis, and imaging were performed as detailed in Supplemental Information. Shown are representative images from at minimum n = 5 mice per treatment group. For rat studies, n=3 per treatment. Quantified data shown are group mean values ± SEM. References cited in the supplementary information.[47, 48, 49, 50, 51]

Supplementary Material

Refer to Web version on PubMed Central for supplementary material.

Acknowledgments

This work was supported by the Juvenile Diabetes Research Foundation (JDRF) (Grant 17-2007-1063), and Leona M. and Harry B. Helmsley Charitable Trust Foundation (Grant 09PG-T1D027), National Institutes of Health (Grants EB000244, EB000351, DE013023 and CA151884), Koch Institute Support (core) Grant P30-CA14051 from the National Cancer Institute, and through a generous gift from the Tayebati Family Foundation. OV was supported by JDRF and DOD/CDMRP postdoctoral fellowships (Grants 3-2013-178 and W81XWH-13-1-0215, respectively). J.O. is supported by the National Institutes of Health (NIH/NIDDK) R01DK091526 and the Chicago Diabetes Project, J.M.E. is supported by the American Diabetes Association (ADA) Clinical Scientist Training Award (7-12-CST-03), and the American Society of Transplant Surgeons (ASTS) Presidential Student Mentor Award. The authors would like to acknowledge the use of resources at the Koch Institute Swanson Biotechnology Center for technical support, specifically, the Hope Babette Tang Histology, Microscopy, Flow Cytometry, and Animal Imaging and pre-clinical testing core facilities. We acknowledge the use of imaging resources at the W.M. Keck Biological Imaging Facility (Whitehead Institute), and assistance from Dr. Wendy Salmon. We thank Drs. Roman Bogorad and Kathryn Whitehead for helpful discussions and feedback on the manuscript.

References

1. Kearney CJ, Mooney DJ. Macroscale delivery systems for molecular and cellular payloads. Nature materials. 2013; 12(11):1004–1017.
2. Farra R, Sheppard NF Jr, McCabe L, Neer RM, Anderson JM, Santini JT Jr, et al. First-in-human testing of a wirelessly controlled drug delivery microchip. Sci Transl Med. 2012; 4(122):122ra121.
3. Nichols SP, Koh A, Storm WL, Shin JH, Schoenfisch MH. Biocompatible materials for continuous glucose monitoring devices. Chemical reviews. 2013; 113(4):2528–2549. [PubMed: 23387395]
4. Rosen MR, Robinson RB, Brink PR, Cohen IS. The road to biological pacing. Nat Rev Cardiol. 2011; 8(11):656–666. [PubMed: 21844918]
5. Hubbell JA, Langer R. Translating materials design to the clinic. Nature materials. 2013; 12(11): 963–966.
6. Franz S, Rammelt S, Scharnweber D, Simon JC. Immune responses to implants – a review of the implications for the design of immunomodulatory biomaterials. Biomaterials. 2011; 32(28):6692–6709. [PubMed: 21715002]
7. Anderson JM, Rodriguez A, Chang DT. Foreign body reaction to biomaterials. Semin Immunol. 2008; 20(2):86–100. [PubMed: 18162407]

8. Williams DF. On the mechanisms of biocompatibility. Biomaterials. 2008; 29(20):2941–2953. [PubMed: 18440630]
9. Ratner BD. Reducing capsular thickness and enhancing angiogenesis around implant drug release systems. J Control Release. 2002; 78(1–3):211–218. [PubMed: 11772462]
10. Bryers JD, Giachelli CM, Ratner BD. Engineering biomaterials to integrate and heal: the biocompatibility paradigm shifts. Biotechnol Bioeng. 2012; 109(8):1898–1911. [PubMed: 22592568]
11. Zhang L, Cao Z, Bai T, Carr L, Ella-Menye JR, Irvin C, et al. Zwitterionic hydrogels implanted in mice resist the foreign-body reaction. Nat Biotechnol. 2013; 31(6):553–556. [PubMed: 23666011]
12. Smith RS, Zhang Z, Bouchard M, Li J, Lapp HS, Brotske GR, et al. Vascular catheters with a nonleaching poly-sulfobetaine surface modification reduce thrombus formation and microbial attachment. Sci Transl Med. 2012; 4(153):153ra132.
13. Ma M, Liu WF, Hill PS, Bratlie KM, Siegwart DJ, Chin J, et al. Development of cationic polymer coatings to regulate foreign-body responses. Advanced materials. 2011; 23(24):H189–194. [PubMed: 21567481]
14. Rodriguez PL, Harada T, Christian DA, Pantano DA, Tsai RK, Discher DE. Minimal “Self” peptides that inhibit phagocytic clearance and enhance delivery of nanoparticles. Science. 2013; 339(6122):971–975. [PubMed: 23430657]
15. Kim YK, Que R, Wang SW, Liu WF. Modification of Biomaterials with a Self-Protein Inhibits the Macrophage Response. Advanced healthcare materials. 2014
16. Madden LR, Mortisen DJ, Sussman EM, Dupras SK, Fugate JA, Cuy JL, et al. Proangiogenic scaffolds as functional templates for cardiac tissue engineering. Proceedings of the National Academy of Sciences of the United States of America. 2010; 107(34):15211–15216. [PubMed: 20696917]
17. Kusaka T, Nakayama M, Nakamura K, Ishimiya M, Furusawa E, Ogasawara K. Effect of silica particle size on macrophage inflammatory responses. PloS one. 2014; 9(3):e92634. [PubMed: 24681489]
18. Zandstra J, Hiemstra C, Petersen AH, Zuidema J, van Beuge MM, Rodriguez S, et al. Microsphere size influences the foreign body reaction. European cells & materials. 2014; 28:335–347. [PubMed: 25350249]
19. Matlaga BF, Yasenchak LP, Salthouse TN. Tissue response to implanted polymers: the significance of sample shape. Journal of biomedical materials research. 1976; 10(3):391–397. [PubMed: 1270456]
20. Salthouse TN. Some aspects of macrophage behavior at the implant interface. Journal of biomedical materials research. 1984; 18(4):395–401. [PubMed: 6234318]
21. Helton KL, Ratner BD, Wisniewski NA. Biomechanics of the sensor-tissue interface-effects of motion, pressure, and design on sensor performance and the foreign body response-part I: theoretical framework. Journal of diabetes science and technology. 2011; 5(3):632–646. [PubMed: 21722578]
22. Brauker JH, Carr-Brendel VE, Martinson LA, Crudele J, Johnston WD, Johnson RC. Neovascularization of synthetic membranes directed by membrane microarchitecture. Journal of biomedical materials research. 1995; 29(12):1517–1524. [PubMed: 8600142]
23. Ward WK, Slobodzian EP, Tiekotter KL, Wood MD. The effect of microgeometry, implant thickness and polyurethane chemistry on the foreign body response to subcutaneous implants. Biomaterials. 2002; 23(21):4185–4192. [PubMed: 12194521]
24. Lee KY, Mooney DJ. Alginate: properties and biomedical applications. Progress in polymer science. 2012; 37(1):106–126. [PubMed: 22125349]
25. Whelehan M, Marison IW. Microencapsulation using vibrating technology. Journal of microencapsulation. 2011; 28(8):669–688. [PubMed: 22047545]
26. Lim F, Sun AM. Microencapsulated islets as bioartificial endocrine pancreas. Science. 1980; 210(4472):908–910. [PubMed: 6776628]
27. Scharp DW, Marchetti P. Encapsulated islets for diabetes therapy: history, current progress, and critical issues requiring solution. Advanced drug delivery reviews. 2014:67–68. 35–73. [PubMed: 24361391]

28. Dolgin E. Encapsulate this. Nat Med. 2014; 20(1):9–11. [PubMed: 24398953]
29. Dang TT, Bratlie KM, Bogatyrev SR, Chen XY, Langer R, Anderson DG. Spatiotemporal effects of a controlled-release anti-inflammatory drug on the cellular dynamics of host response. Biomaterials. 2011; 32(19):4464–4470. [PubMed: 21429573]
30. King A, Sandler S, Andersson A. The effect of host factors and capsule composition on the cellular overgrowth on implanted alginate capsules. Journal of biomedical materials research. 2001; 57(3): 374–383. [PubMed: 11523032]
31. Kolb M, Bonniaud P, Galt T, Sime PJ, Kelly MM, Margetts PJ, et al. Differences in the fibrogenic response after transfer of active transforming growth factor-beta1 gene to lungs of “fibrosis-prone” and “fibrosis-resistant” mouse strains. Am J Respir Cell Mol Biol. 2002; 27(2):141–150. [PubMed: 12151305]
32. Lekka M, Sainz-Serp D, Kulik AJ, Wandrey C. Hydrogel microspheres: influence of chemical composition on surface morphology, local elastic properties, and bulk mechanical characteristics. Langmuir : the ACS journal of surfaces and colloids. 2004; 20(23):9968–9977. [PubMed: 15518482]
33. Shellenberger K, Logan BE. Effect of molecular scale roughness of glass beads on colloidal and bacterial deposition. Environmental science & technology. 2002; 36(2):184–189. [PubMed: 11827052]
34. Papajova E, Bujdos M, Chorvat D, Stach M, Lacik I. Method for preparation of planar alginate hydrogels by external gelling using an aerosol of gelling solution. Carbohydrate polymers. 2012; 90(1):472–482. [PubMed: 24751067]
35. Fujie T, Ricotti L, Desii A, Menciassi A, Dario P, Mattoli V. Evaluation of substrata effect on cell adhesion properties using freestanding poly(L-lactic acid) nanosheets. Langmuir : the ACS journal of surfaces and colloids. 2011; 27(21):13173–13182. [PubMed: 21913651]
36. Qi M, Lacik I, Kollarikova G, Strand BL, Formo K, Wang Y, et al. A recommended laparoscopic procedure for implantation of microcapsules in the peritoneal cavity of non-human primates. The Journal of surgical research. 2011; 168(1):e117–123. [PubMed: 21435661]
37. Dang TT, Thai AV, Cohen J, Slosberg JE, Siniakowicz K, Doloff JC, et al. Enhanced function of immuno-isolated islets in diabetes therapy by co-encapsulation with an anti-inflammatory drug. Biomaterials. 2013; 34(23):5792–5801. [PubMed: 23660251]
38. de Groot M, Schuurs TA, van Schilfgaarde R. Causes of limited survival of microencapsulated pancreatic islet grafts. The Journal of surgical research. 2004; 121(1):141–150. [PubMed: 15313388]
39. Strand BL, Gaserod O, Kulseng B, Espevik T, Skjak-Baek G. Alginate-polylysine-alginate microcapsules: effect of size reduction on capsule properties. Journal of microencapsulation. 2002; 19(5):615–630. [PubMed: 12433304]
40. Robitaille R, Pariseau JF, Leblond FA, Lamoureux M, Lepage Y, Halle JP. Studies on small (<350 microm) alginate-poly-L-lysine microcapsules. III. Biocompatibility Of smaller versus standard microcapsules. Journal of biomedical materials research. 1999; 44(1):116–120. [PubMed: 10397911]
41. Shi C, Pamer EG. Monocyte recruitment during infection and inflammation. Nat Rev Immunol. 2011; 11(11):762–774. [PubMed: 21984070]
42. Burnett SH, Kershen EJ, Zhang J, Zeng L, Straley SC, Kaplan AM, et al. Conditional macrophage ablation in transgenic mice expressing a Fas-based suicide gene. Journal of leukocyte biology. 2004; 75(4):612–623. [PubMed: 14726498]
43. Gordon S. Alternative activation of macrophages. Nat Rev Immunol. 2003; 3(1):23–35. [PubMed: 12511873]
44. Mosser DM, Edwards JP. Exploring the full spectrum of macrophage activation. Nat Rev Immunol. 2008; 8(12):958–969. [PubMed: 19029990]
45. Murray PJ, Allen JE, Biswas SK, Fisher EA, Gilroy DW, Goerdt S, et al. Macrophage activation and polarization: nomenclature and experimental guidelines. Immunity. 2014; 41(1):14–20. [PubMed: 25035950]
46. Gordon S, Martinez FO. Alternative activation of macrophages: mechanism and functions. Immunity. 2010; 32(5):593–604. [PubMed: 20510870]

47. Lacy PE, Kostianovsky M. Method for the isolation of intact islets of Langerhans from the rat pancreas. Diabetes. 1967; 16(1):35–39. [PubMed: 5333500]

48. Morch YA, Donati I, Strand BL, Skjak-Braek G. Effect of Ca2+, Ba2+, and Sr2+ on alginate microbeads. Biomacromolecules. 2006; 7(5):1471–1480. [PubMed: 16677028]

49. Ricordi C, Gray DW, Hering BJ, Kaufman DB, Warnock GL, Kneteman NM, et al. Islet isolation assessment in man and large animals. Acta Diabetol Lat. 1990; 27(3):185–195. [PubMed: 2075782]

50. Adewola AF, Lee D, Harvat T, Mohammed J, Eddington DT, Oberholzer J, et al. Microfluidic perifusion and imaging device for multi-parametric islet function assessment. Biomed Microdevices. 2010; 12(3):409–417. [PubMed: 20300858]

51. Keizer J, Magnus G. ATP-sensitive potassium channel and bursting in the pancreatic beta cell. A theoretical study. Biophys J. 1989; 56(2):229–242. [PubMed: 2673420]

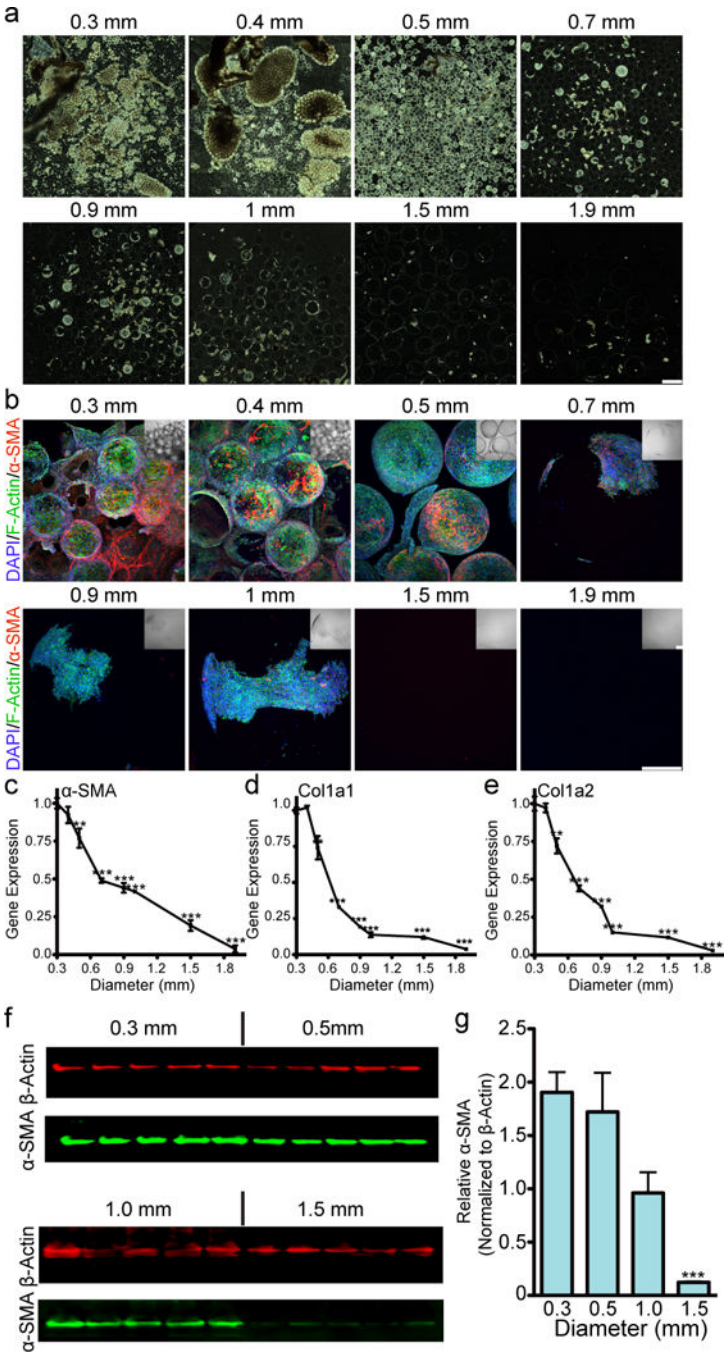

Figure 1. Increasing alginate sphere size results in reduced cellular deposition and fibrosis formation on the spheres

SLG20 alginate spheres (0.5 ml in volume) of 8 different sizes (0.3, 0.4, 0.5, 0.6, 0.7, 1, 1.5, and 1.9 mm) were implanted into the intraperitoneal space of C57BL/6 mice, where they were retained for 14 days and analyzed for degree of fibrosis upon retrieval. Dark field phase contrast images obtained from retrieved spheres reveal a significant decrease in level of cellular overgrowth with increase in sphere size (**a**); scale bar = 2mm). Z-stacked confocal images of retrieved spheres immunofluorescence stained with DAPI (highlighting

cellular nuclei), phalloidin (Highlighting F-actin), and α-Smooth Muscle Actin (α-SMA, Myofibroblast cells) (**b**); Scale bar = 300μm). q-PCR based expression analysis of fibrotic markers α-SMA (**c**), Collagen 1a1 (**d**, Col1a1), and Collagen 1a2 (**e**, Col1a2) directly on the 8 various sized (0.3, 0.4, 0.5, 0.7, 0.9, 1, 1.5, 1.9 mm) spheres plotted normalized to relative expression levels on 300 μm sized spheres. Semi-quantitative western blot analysis of analysis of α-SMA expression in cell overgrowth from on microspheres (1–5 labeling of bands corresponds to individual mice) (**f**). Plot of analyzed band intensities from western blot images shown in f (**g**). Error bars, mean ± SEM. N = 5 mice per treatment. All experiments were performed at least three times. qPCR and western blot statistical analysis: one-way ANOVA with Bonferroni multiple comparison correction *: $p < 0.05$, **: $p < 0.001$, and ***: $p < 0.0001$.

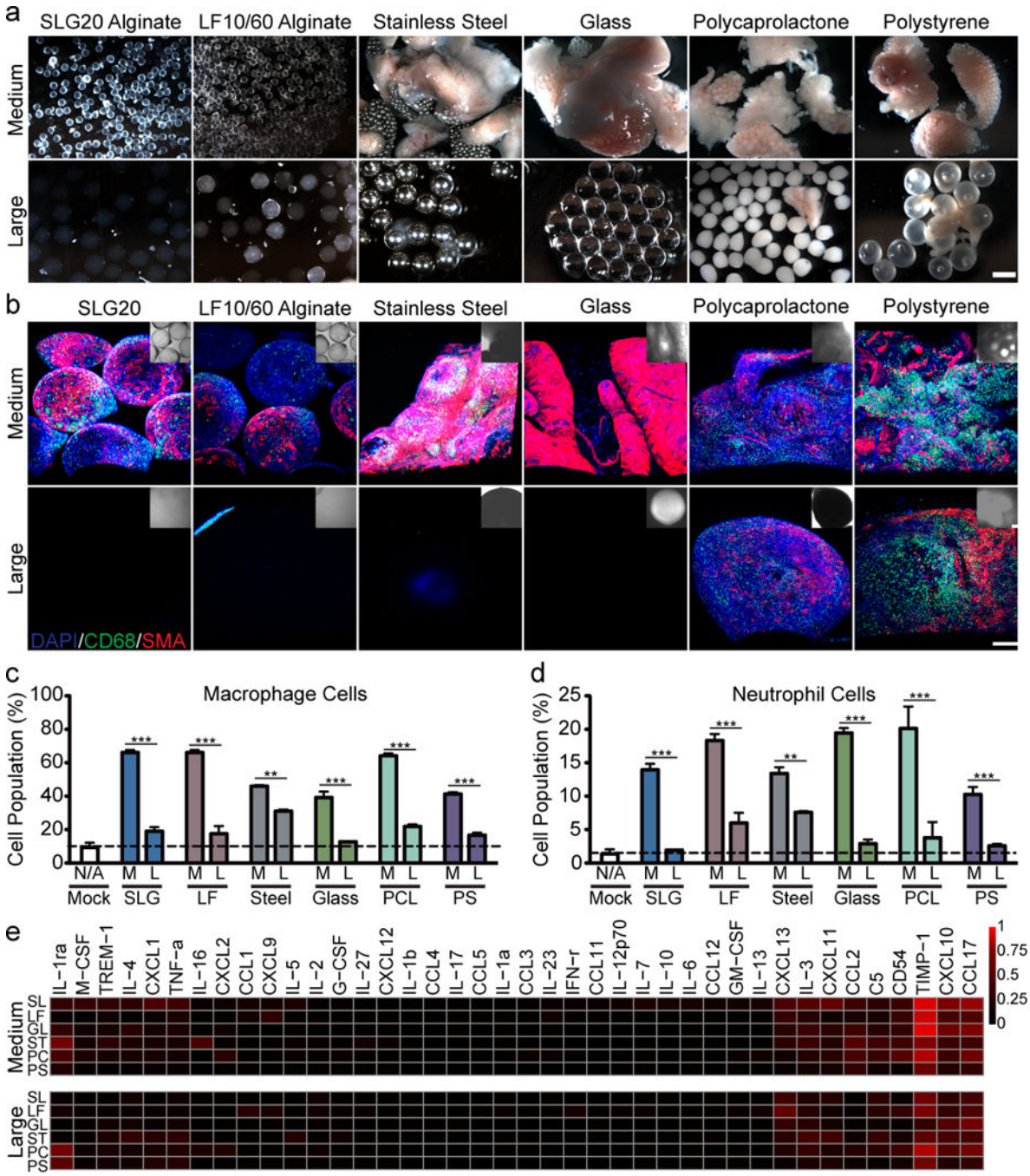

Figure 2. Increasing the spherical diameter of a variety of materials including, hydrogels, ceramics, metals, and plastics results in reduced foreign body responses

Bright-field images obtained from retrieved medium (0.5 mm) and large (1.5–2 mm) sized versions of SLG20 alginate, LF10/60 alginate (endotoxin containing), glass, and polystyrene 14 days post intraperitoneal implant into C57BL/6 mice (**a**); Scale bar = 2 mm. Panel of representative immunofluorescence Z-stacked confocal images of materials stained for cell nuclei (DAPI, blue), macrophages (CD68, green) and fibrosis-associated activated myofibroblasts (α-SMA, red) (**b**); scale bar = 300 μm. Flow analysis, using specific markers

for responding host macrophage (**c**) neutrophils (**d**); Mock = surgery and PBS only injection, SLG = SLG20 alginate, LF = LF10/60 alginate (endotoxin containing), PCL = polycaprolactone, and PS= polystyrene. Elispot multiplexed based cytokine array profiling of inflammatory cytokine protein production in response to implanted materials (e); SL = SLG20 alginate, LF = LF10/60 alginate (endotoxin containing), ST= stainless steel, GL = glass PC = polcaprolactone, and PS= polystyrene. Error bars, mean ± SEM. N = 5 mice per treatment. All experiments were performed at least three times. FACS size comparisons were performed by unpaired, two-tailed t-test *: $p < 0.05$, **: $p < 0.001$, and ***: $p < 0.0001$.

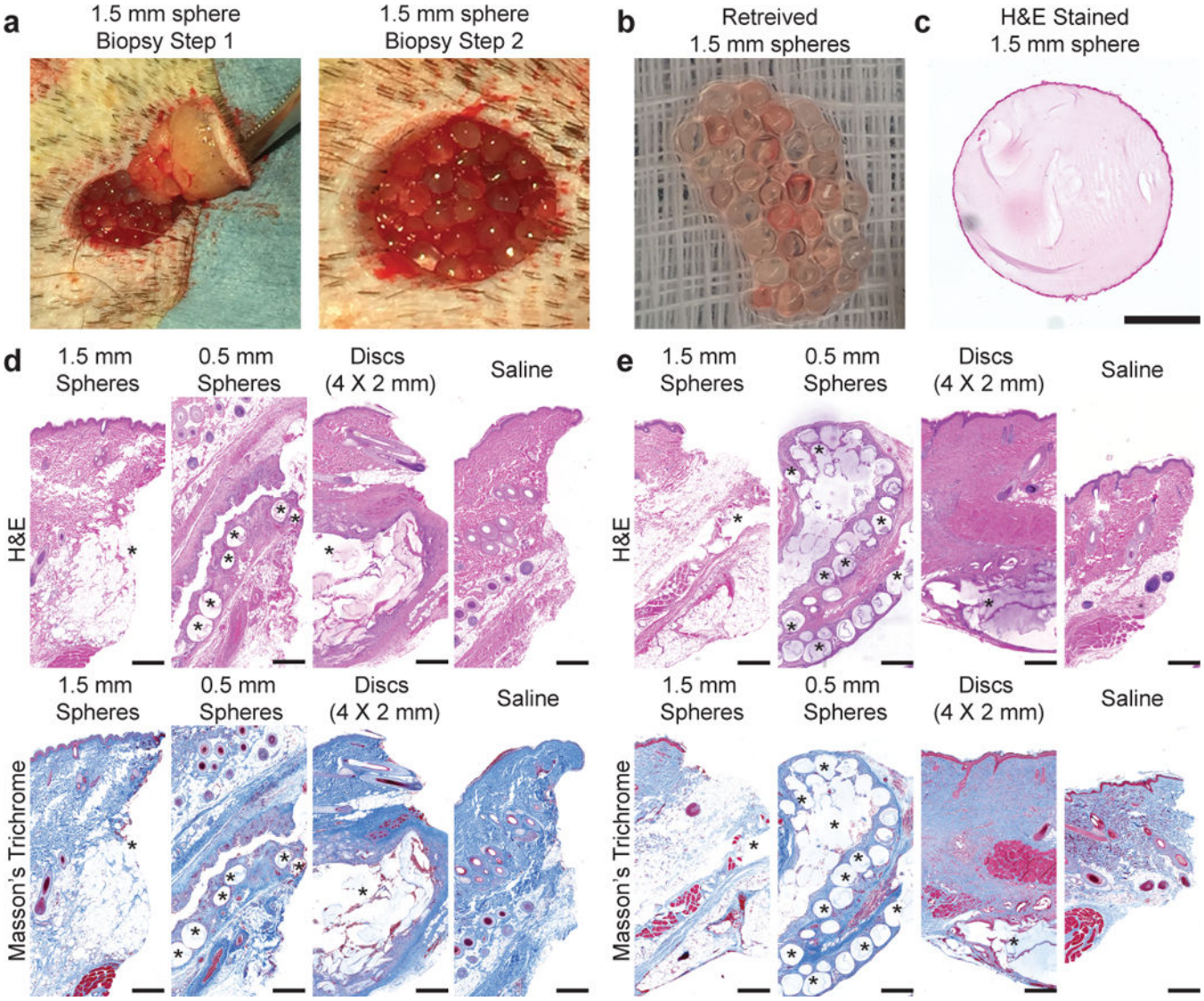

Figure 3. Comparing the size and shape dependence effects of fibrosis formation on to alginate hydrogels implanted in the subcutaneous dorsal region of non-human primates

Large 1.5 mm-sized spheres of SLG20 hydrogels implanted subcutaneously in the dorsal region of cynomolgus macaques resist fibrosis, while small spheres (0.5 mm sized) and cylinders (4 mm in diameter and 2 mm in height) become fibrotic. After 14 days, biopsy punches were used to excise implanted materials/peripheral host tissue; upon incision we observed that the large SLG20 alginate spheres were not embedded in host tissue and freely dissociated from the implant site (**a**). The retrieved large SLG20 hydrogels visually appear to be transparent and void of cellular deposition (**b**), which was also confirmed using H&E stained histological analysis (**c**); Scale bar = 500 μm. H&E and Masson's Trichrome stained histological sections of excised tissue at 14 days (**d**, Scale bar = 500 μm), and 28 days (**e**, Scale bar = 500 μm) post-implantation with SLG20 alginate hydrogels formed into large spheres (1.5 mm in diameter), medium sized spheres (0.5 mm in diameter) or cylinders (4 mm in diameter and 1 mm in height), and as well a control saline alone injection (* in

images demarks implanted materials). N = 2 for saline and discs; N = 4 for both 0.5 and 1.5 mm sphere groups. These experiments were performed once.

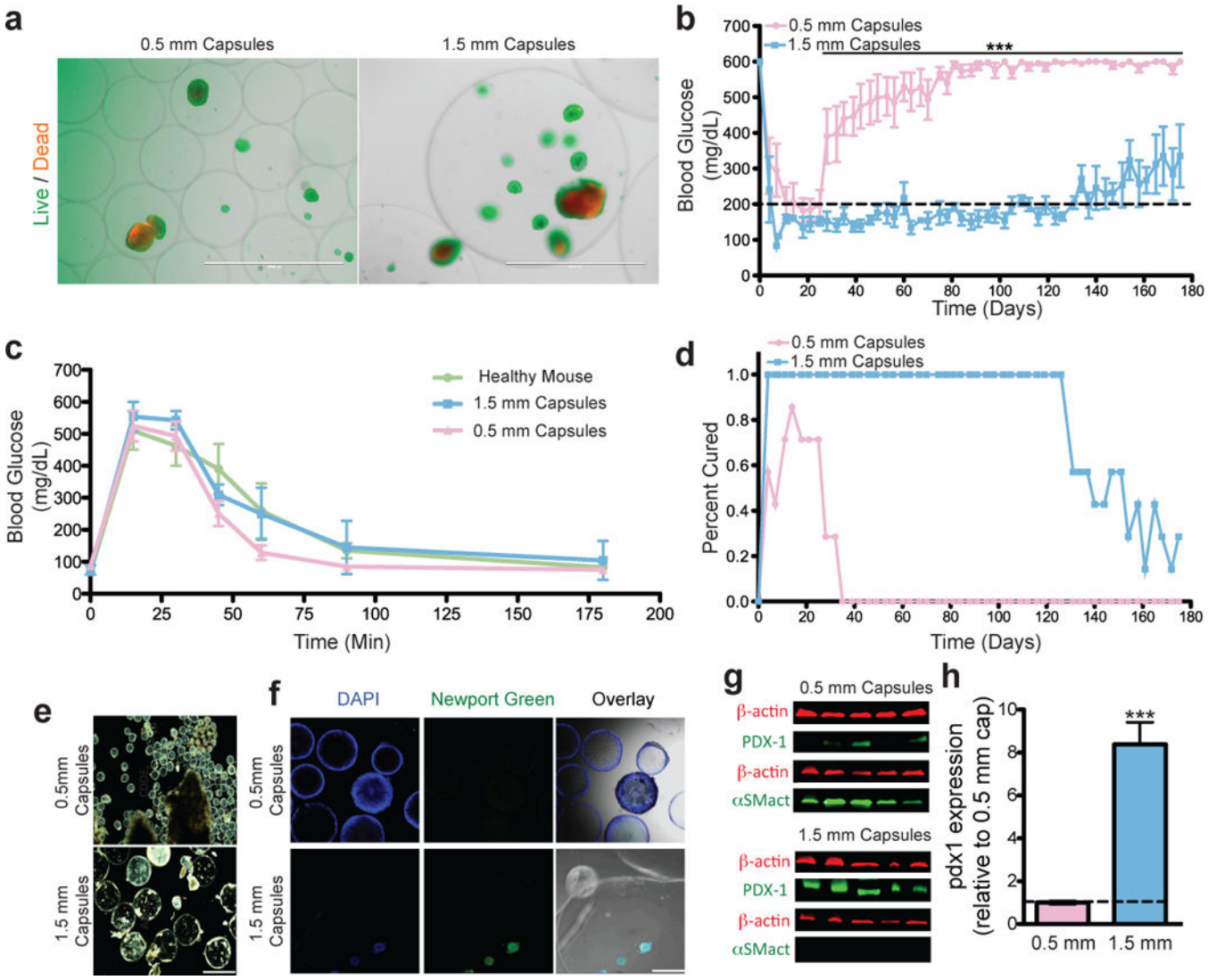

Figure 4. Comparison of 0.5 mm and 1.5 mm alginate capsules encapsulating rat islets (500 IE's) in curing STZ-induced C57BL/6 diabetic mice

Live/dead staining confirming viability of islet cells post-encapsulation for large 1.5 mm as well as standard 0.5 mm capsules (**a**); Scale bar = 1000 μm. Blood glucose curves showing prolonged normoglycemia with large 1.5 mm diameter hydrogel alginate capsules, but only short-lived success with standard 0.5 mm diameter capsules (**b**). In vivo Glucose Tolerance Test (iv GTT) of healthy mice and diabetic mice 7 days post-transplantation with rat islets encapsulated in standard (0.5 mm) or large sized capsules (1.5 mm) shows no significant delays in BG correction as a function of capsule geometry (**c**). Kaplan-Meier plot showing fraction of cured STZ-C57BL/6 mice after being transplanted with either 0.5 mm or 1.5 mm diameter capsules, containing 500 IE's of primary rat islets (**d**). Representative dark field phase contrast images of retrieved 0.5 mm or 1.5 mm alginate islet-containing capsules 6 months after transplantation show higher levels of cellular overgrowth on 0.5 mm capsules (**e**); Scale bar = 2000 μm. Confocal imaging panel showing nuclear DAPI (*left*), Newport green (islet marker, *center*), and overlay with bright field images of visible capsules (*right*)

(**f**); Scale bar = 300 μm. Rat PDX-1 and host alpha smooth muscle actin expression from capsules retrieved from STZ treated mice 175 days post-transplant. As a reference, β-actin expression levels are also shown (**g**). qPCR analysis of rat islet marker Pdx1 expression in retrieved 0.5 or 1.5 mm alginate capsules (**h**). Error bars, mean ± SEM. N = 5 mice per treatment. All experiments were performed at least two or three times. qPCR statistical analysis: one-way ANOVA with Bonferroni multiple comparison correction *: $p < 0.0001$.

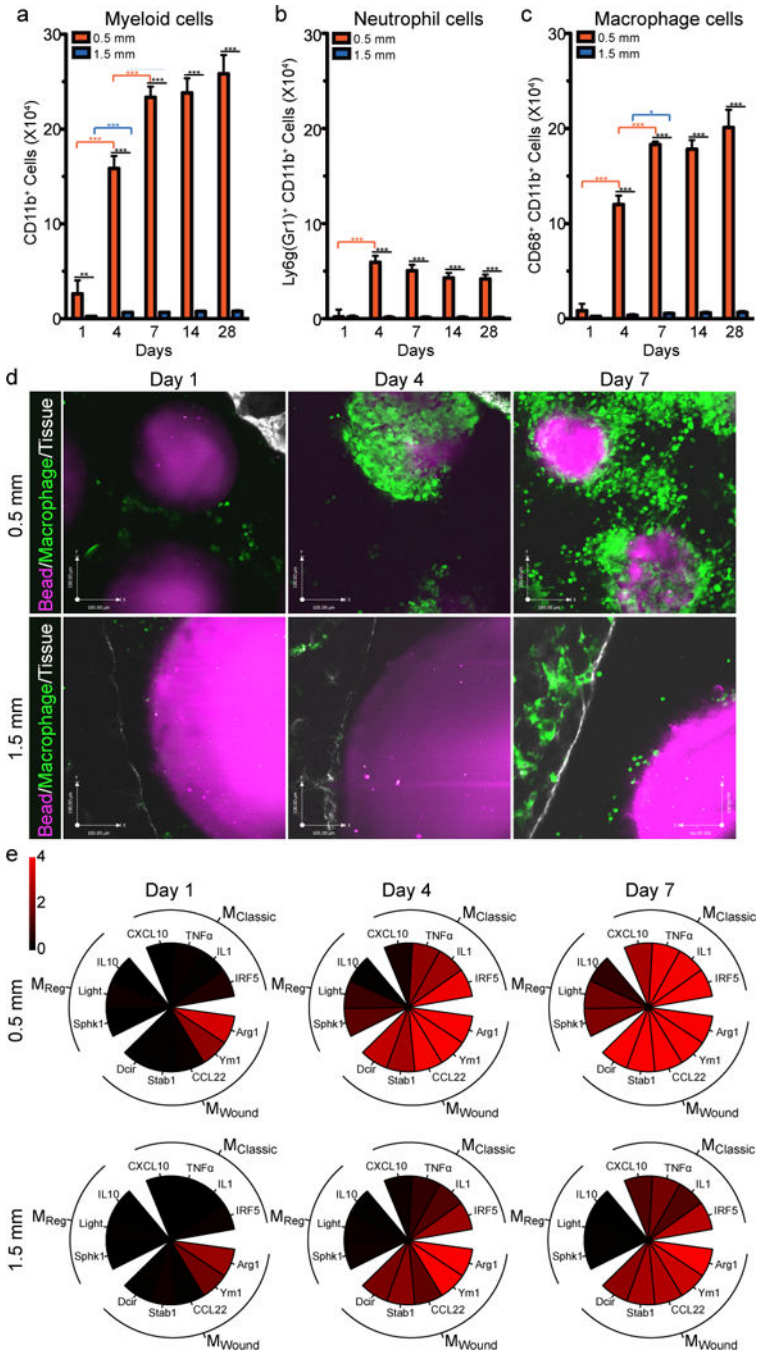

Figure 5. Kinetic profiling of host response to SLG20 alginate microspheres of 0.5 and 1.5 mm sizes in diameter

Flow analysis, using specific markers for responding host innate immune myeloid (**a**), neutrophil (**b**), and macrophage cells (**c**) at 1, 4, 7, 14, and 28 days post-implantation. In vivo intravital imaging of macrophage behavior and accumulation at 1, 4, or 7 days post-implantation (**d**). NanoString-based analysis for expression of macrophage phenotype markers analyzed from deposited cell RNA extracts at 1, 4, and 7 days post-implant, presented on a base 2 logarithmic scale (**e**). Error bars, mean ± SEM. For FACS analysis N

= 5 mice per treatment, for intravital imaging: N = 3 mice per treatment, for Nanostring analysis N = 4 per treatment. FACS and intravital imaging experiments were performed twice and nanostring analysis was performed once. FACS size comparisons were performed by unpaired, two-tailed t-test *: $p < 0.05$, **: $p < 0.001$, and ***: $p < 0.0001$. For nanostring statistical analyses see supplemental methods.